Technical Note

Motion Corrected Free-Breathing Delayed-Enhancement Imaging of Myocardial Infarction Using Nonrigid Registration

Maria J. Ledesma-Carbayo, PhD,[1,2] Peter Kellman, PhD,[1]* Andrew E. Arai MD,[1] and Elliot R. McVeigh, PhD[1]

Purpose: To develop and test an automatic free-breathing, delayed enhancement imaging method with improved image signal-to-noise ratio (SNR).

Materials and Methods: The proposed approach uses free-breathing, inversion-recovery single-shot fast imaging with steady precession (FISP) delayed-enhancement with respiratory motion compensation based on nonrigid image registration. Motion-corrected averaging is used to enhance SNR.

Results: Fully automatic, nonrigid registration was compared to previously validated rigid body registration that required user interaction. The performance was measured using the variance of edge positions in intensity profiles through the myocardial infarction (MI) enhanced region and through the right ventricular (RV) wall. Measured variation of the MI edge was 1.16 ± 0.71 mm (N = 6 patients; mean $\pm$ SD) for rigid body and 1.08 ± 0.76 mm for nonrigid registration (no significant difference). On the other hand, significant improvement ($P < 0.005$) was found in the measurements at the RV edge where the SD was 2.06 ± 0.56 mm for rigid body and 0.59 ± 0.22 mm for nonrigid registration.

Conclusion: The proposed approach achieves delayed enhancement images with high resolution and SNR without requiring a breathhold. Motion correction of free-breathing delayed-enhancement imaging using nonrigid image registration may be implemented in a fully automatic fashion and performs uniformly well across the full field of view (FOV).

Key Words: delayed enhancement; myocardial infarction; free-breathing; motion correction; nonrigid registration; SENSE
J. Magn. Reson. Imaging 2007;26:184–190.
© 2007 Wiley-Liss, Inc.

MYOCARDIAL VIABILITY assessment using gadolinium diethylenetriamine pentaacetic acid (Gd-DTPA) delayed-enhancement MRI is gaining clinical acceptance (1,2). Imaging based on inversion recovery with breath-held, segmented turbo-fast low-angle shot (FLASH) readout provides high spatial resolution and good contrast (3), and is widely considered the conventional acquisition method (4). Using a segmented acquisition requires a number of breathholds to image the heart. Single-shot imaging with true-fast imaging with steady precession (FISP) readout (5) may be conducted during free-breathing, which provides an alternative for cases in which patients cannot tolerate (5) breathholding. Single-shot imaging is also an attractive protocol for reducing scan time (6). Single-shot true-FISP inversion recovery has been validated against conventional inversion recovery segmented turbo-FLASH for assessment of myocardial infarction (MI) at both 1.5 and 3T (7,8).

Respiratory motion-corrected averaging of multiple images acquired while free-breathing may be used to substantially improve the image quality (5). The motivation for motion-corrected averaging with single-shot delayed-enhancement imaging is to improve the signal-to-noise ratio (SNR). Delayed enhancement images are typically acquired during mid diastasis to minimize blurring due to cardiac motion. The temporal resolution of single-shot true-FISP images is not as good as segmented acquisitions; therefore, a somewhat reduced matrix size is frequently accepted (9). However, reduced spatial resolution may reduce the sensitivity to smaller MIs (10). Parallel imaging may be applied to single-shot true-FISP delayed-enhancement to improve the temporal resolution without reducing the spatial resolution (5) at the expense of reduced SNR. Averaging may be used to offset the loss in SNR incurred due to parallel

imaging, thereby achieving the quality of conventional segmented breathheld imaging using a free-breathing protocol.

In prior work, rigid body image registration was used to correct respiratory motion in the heart region, based on a user-defined bounding box (5). In this work, non-rigid body image registration is used to correct respiratory motion across the full field-of-view (FOV). Previous literature shows that nonrigid transformations are actually necessary to account for all the deformation induced in the heart through the respiration process (11–14). Both affine (11,12) and nonrigid schemes (13,14) have been previously proposed in non-contrast-enhanced image data. In this study we aim to prove the validity of this type of approach on delayed enhancement data acquired with free-breathing. The main advantages of using nonrigid body correction are the ability to perform the entire process automatically, and improved motion correction across the full FOV. After applying nonrigid body motion correction, both the right ventricular (RV) and left ventricular (LV) imaging may be simultaneously corrected, proving a better fit of the transformation model to the actual heart deformation induced by breathing.

MATERIALS AND METHODS

Imaging

In this study we used the same data used in our prior work (5) as it was validated vs. breathheld segmented turbo-FLASH data. Delayed-enhancement imaging was performed in patients with chronic MI under a clinical research protocol approved by our Institutional Review Board, with prior informed consent. Images are usually acquired between 10 and 30 minutes after administering a double dose (0.2 mmol/kg) of contrast agent (Gadopentetate dimeglumine, Magnevist; Berlex). Experiments were conducted using a 1.5-T Siemens Sonata MR imaging system. Custom modification to the Siemens product inversion-recovery true-FISP sequence and phase-sensitive inversion recovery (PSIR) reconstruction software was made to incorporate parallel imaging using sensitivity encoding (SENSE) as previously described (5). Raw data including prescan noise was acquired for all scans, and images were reconstructed offline.

Short-axis slices through the MI region were acquired in $N = 6$ patients with chronic MI and long-axis images were acquired in two of the patients. The mean age of the patients was 53.2 ± 10.7 years (mean ± SD). The mean weight of the patients was 202 ± 27 lbs. (mean ± SD). The mean heart rate of the patients was 61.5 ± 10.3 bpm (mean ± SD). All patients were male. For each slice imaged, data was acquired for multiple ($N \approx 30$) free-breathing repetitions.

Motion Correction

Respiratory motion compensation was achieved performing independent nonrigid registration processes of a reference frame with respect to all the other frames in the complete set of acquired images. Unlike using rigid registration, which would require a user-defined

bounding region, the full FOV was used. Therefore, user interaction was not required in the process. As a result, the full FOV is motion-compensated and a motion-corrected average image is improved homogeneously across the full FOV.

Each independent registration step consists of an optimization procedure that minimizes a similarity measure of the two images to find the best transformation that maps a given frame into the frame of reference. The chosen similarity measure is the sum of squared differences, which is a simple criterion with fast computation that enables a smooth and robust optimization. A regularization term was added to the criterion to overcome some of the intrinsic difficulties of the registration process such as artifacts and noise.

The optimization used a variation of the Marquart-Levenverg nonlinear least squares (15). Speed and robustness are guaranteed using a multiresolution approach, both in the image and transformation space, which creates an optimal pyramid of subsampled images (16) and solves the problem by following a coarse to fine strategy.

The transformation between the target and reference frame was defined as a linear combination of B-spline basis functions, located in a regular grid defined on the image space (15,17,18). The density of the grid determines the final rigidity of the transformation (the denser grid the more flexible the transformation) and therefore determines the number of parameters to be optimized. The spline transformation model has the advantage of good accuracy and intrinsic smoothness of the solution thereby providing a very good balance between global and local transformations by appropriately tuning the density of the B-spline grid.

Spline interpolation was also used to provide a continuous version of the discrete images; providing an excellent framework to find a subpixel solution and to analytically compute the derivatives needed in the optimization and regularization processes.

To choose the optimal parameters for the particular application in this work, we performed a set of initial tests. Three different transformation grid spacings were tested: 5, 10, and 20 pixels. The evaluation criterion was to provide the least mean squared error (MSE) along the whole motion-compensated sequence. As a result, cubic B-splines with a grid spacing set to 5×5 pixels (5 pixels ~ 6.8 mm) provided the best results and were used to represent the deformation. Cubic B-splines were also used for image interpolation and for providing a continuous representation. The multiscale processing scheme was set at three levels with successive levels having half the size in each dimension. Regularization was used in all the cases and found to make the solution more stable.

Registration was performed on the images prior to the surface coil intensity correction (SCIC) and the resulting motion parameters from the nonrigid registration were then applied to the SCIC images. This scheme was found to be more effective than applying the registration directly to the intensity-corrected images, since these images have high values in noise-only regions that could degrade the intensity-based registration outcome.

For the short-axis images, in which there was little through-plane motion, the reference image was simply chosen as the first image in the series of repeated measurements. For the long-axis images, because of the significant through-plane motion, we performed a MSE strategy to select the best three consecutive reference images, corresponding to different respiratory positions. The selection of these three frames was done prior to registration by computing the MSE between every frame as a reference and all the other frames in the series. Then, a MSE sorting was performed for each frame as a reference and the three consecutive frames with the least accumulated MSE along the N first sorted images were chosen, where N was approximately 30% of the entire number of images acquired during free-breathing. Each of these reference images was registered to those N images that had the smallest corresponding MSE prior to registration.

Motion-corrected images were averaged to enhance SNR. Approximately 30 free-breathing frames (60 heartbeats) were acquired. For the short-axis images, all the frames were used to produce an averaged image. For the long-axis images, three output-averaged images were produced—one for each reference image—at different respiratory positions. Each output images was the result of averaging 10 frames with minimum MSE with respect to the corresponding reference image.

Results were compared with rigid body registration as previously described in Ref. 5, based on an image registration algorithm (19) and C-language source code that are open source and freely downloadable. The method used in that case was an intensity-based rigid registration method limited to a bounding box surrounding the left ventricle. Both registration methods are based on the same family of algorithms. However, the main differences are the nonrigid (deformable) vs. the rigid transformation models and the bounding box selection, with respect to the use of the full FOV in the new approach.

Measurements

To assess the performance of the nonrigid registration, the MSE of every deformed frame with respect to the reference was computed and compared to the same measurements obtained for both the nonregistered and rigid-body registered cases. The MSE measurements were confined to the bounding box selected on the rigid registration procedure to make a fair comparison within the area of interest.

The quality of the image registration was assessed by comparing signal intensity profiles both before and after motion compensation using both the rigid body and the nonrigid registration. Two significant edges were selected for each series of images acquired, one at the MI-enhanced area and the other at the RV wall. The sharpness of these edges in the final averaged images (nonregistered, rigid, and nonrigid) was assessed by computing the SD of the edge position (threshold crossing) through the stack of motion-compensated images.

Infarct size was compared between single-shot, inversion-recovery (IR) true-FISP with motion-corrected averaging (eight averages) and conventional segmented IR turbo-FLASH using a previously validated semiautomatic computerized method (20,21) of objective measurement. Infarct size was measured on surface coil intensity-corrected PSIR images. The computerized method required the user to draw both endocardial and epicardial borders to define the myocardial region of interest. The method then contoured high pixel intensity regions using a threshold value corresponding to half of the maximum intensity after first performing a histogram-based thresholding between normal and infarct pixels. Other image processing steps were included for dealing with microvascular obstructions and reducing false-positive infarct pixels.

RESULTS

Short-axis images of the heart for a patient with anteroseptal MI are shown in Fig. 1, comparing resultant

No motion correction   Rigid body motion correction   Deformable body motion correction

non-SCIC
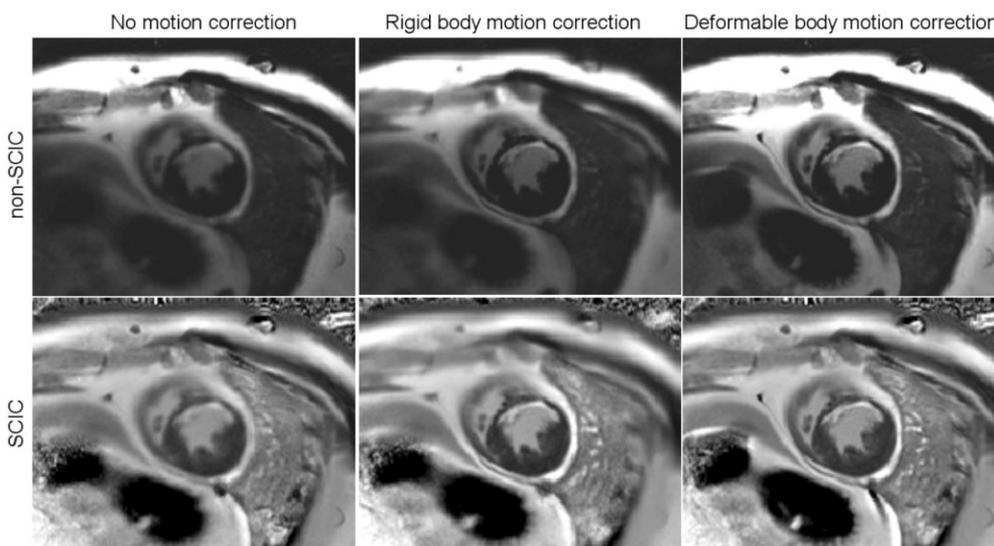
SCIC

Figure 1. Average of 30 images acquired during free breathing for no motion correction (left), rigid body motion correction (middle), and nonrigid body motion correction (right). The bottom row are surface coil intensity corrected (SCIC) and the top row are nonSCIC. Rigid body motion correction uses a user-defined bounding region around the LV to optimize image registration. Nonrigid body motion correction is automatically performed over the full FOV without any user-defined input.

No motion correction   Rigid body motion correction   Deformable body motion correction
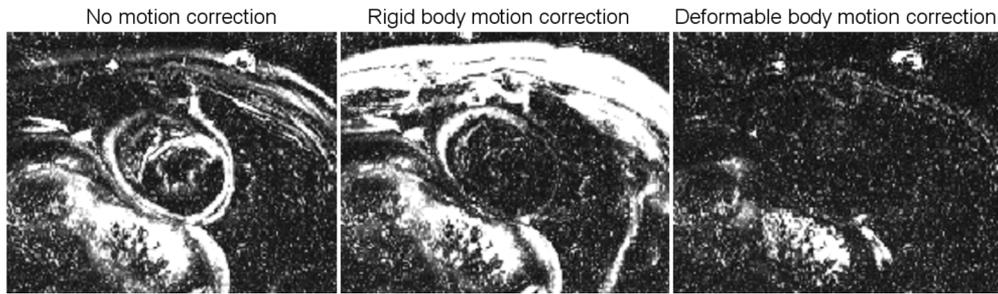
Figure 2. Squared error averaged over time for no motion correction (left), rigid body motion correction (middle), and nonrigid body motion correction (right). Rigid body motion correction has low error within the LV region used for registration but has degraded performance outside the bounding region. Nonrigid motion correction has low error across the full FOV except for areas with inconsistent appearance as a function of time for example peristalsis in the gut.

average images: (left) for no motion correction, (middle) for rigid body motion correction, and (right) for nonrigid body motion correction. In the upper row the non-surface-corrected images are displayed and in the bottom row the SCIC are presented. In this example, the spatial resolution was $1.4 \times 2.3 \times 6$ mm^3 with FOV = 370 × 300 mm^2, and TI = 300 msec. The performance of the nonrigid registration, compensating for the motion over the full FOV is readily observed (chest wall, ribs) as well as a sharper definition of the RV wall and the MI.

Figure 2 shows the MSE accumulated over time for the same cases shown in Fig. 1. Low error is achieved in the area of the left ventricle when rigid motion compensation is applied. Nonrigid motion compensation improves the results further, with lower error across the full FOV except for areas where intensity actually varies over time, for example due to peristalsis in the gut or through-plane motion.

In Fig. 3, the MSE (arbitrary units) vs. time is plotted for the same cases shown in Fig. 1. The calculation is performed within the heart bounding box (inset image) selected for the rigid registration, and results are shown for: the stack of non-motion-corrected images (dashed line), rigid body motion corrected images (dotted line), and nonrigid body motion correction images (solid line). The oscillatory characteristic is due to sampling at close to three images (six heartbeats) per respiratory cycle. Progressive improvement is observed from noncorrected to rigid body motion corrected and further to nonrigid corrected.

The quality assessment of the registration performance was measured using signal intensity profiles. Figure 4 shows the overlayed signal intensity profiles for the 30 noncorrected images (left), rigid body motion corrected images (center), and nonrigid body motion corrected images (right) along a line though the heart shown in inset image, for the case represented in Fig. 1. The left ventricle and MI area are correctly aligned when rigid body transformations are considered. Alignment is better through the full heart area using nonrigid registration, and a great improvement is achieved in the RV area (see arrows in Fig. 4).

Results of the measurements performed to assess the variance of the edge positions show that the SD measured for the position of the MI edge was 1.16 ± 0.71 mm ($N = 6$ patients; mean $\pm$ SD) for rigid body and

1.08 ± 0.76 mm for nonrigid registration (no significant difference). On the other hand, significant improvement ($P < 0.005$) was found in the measurements at the RV edge, where the position SD was 2.06 ± 0.56 mm for rigid body and 0.59 ± 0.22 mm for nonrigid registration.

Long-axis images acquired during free breathing were averaged after motion correction as previously described. Figure 5 shows the three resultant images for each respiratory position, averaging the 10 selected frames (i.e., with lowest MSE with respect to the reference) after nonrigid motion compensation for three consecutive reference frames (in this case, frames numbered 10–12), chosen as previously described. The MI is clearly seen in all of them, but most distinctly in the left column. This approach therefore allows having several images as a result and choosing the one that allows a better quantification of the MI size. In the top row, it can be observed how the nonrigid registration corrects motion over the full FOV.

The comparison of infarct size measurements is shown in Fig. 6, which plots the size for the averaged single-shot true-FISP images vs. conventional, breath-held, segmented turbo-FLASH. The infarct size for averaged images is in close agreement ($y = 0.97x - 5.2$) with the turbo-FLASH method ($R^2 = 0.97$) over a wide
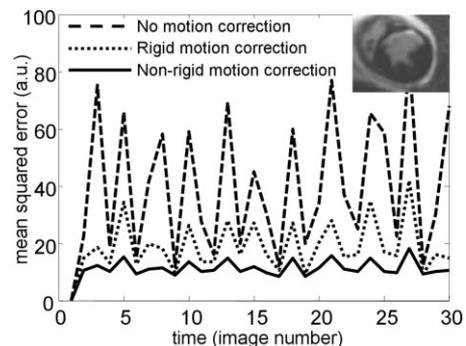
Figure 3. Mean squared error (MSE) vs. time within heart region bounding box (inset image) for no motion correction (dashed line), rigid body motion correction (dotted line), and nonrigid body motion correction (solid line). The oscillation in MSE is due to respiratory motion.
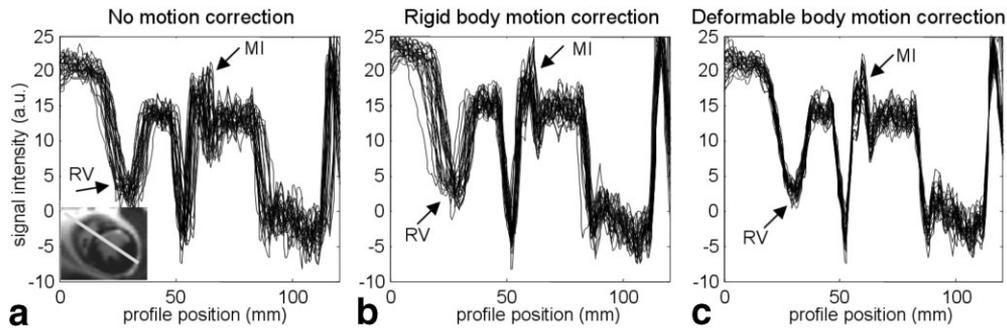
Figure 4. Signal intensity profiles through the heart along line shown in inset image overlayed for 30 images acquired during free-breathing with (**a**) no motion correction (left), (**b**) rigid body motion correction (center), and (**c**) nonrigid body motion correction (right). The intensity profiles are well aligned across the full heart using nonrigid motion correction but have significant motion in RV using rigid body correction.

range of MI sizes. There was no statistically significant difference between the MI size measured using rigid or nonrigid registration methods.

DISCUSSION

Many different nonrigid registration approaches have been proposed in the literature (22). Intensity-based nonrigid registration methods (11,14,23–25) have been used for image-based respiratory motion compensation in several different imaging modalities. We chose to use the sum of squared differences criterion because of its simplicity, fast computation time, and smoothness of the resulting metric. The monomodal nature of our data does not require more complex similarity measurements such as mutual information-based criteria, that

on the other hand may produce a search space with more local minima. The B-spline transformation model was chosen due to its intrinsic smoothness (11,14,25), which accurately represents breathing motion. Another advantage of the parametric B-spline model is its ability to balance the global and local transformations to optimize to the resolution of the data and the amount of expected motion.

Motion compensation based on nonrigid registration performs well for correcting in-plane motion but cannot accurately correct through-plane motion due to respiration or other temporal variations such as peristalsis. This is most evident in the long-axis views, where there is significant through-plane motion due to the location and geometry of the left ventricle and the nature of the respiratory motion. To mitigate this issue, we have pro-
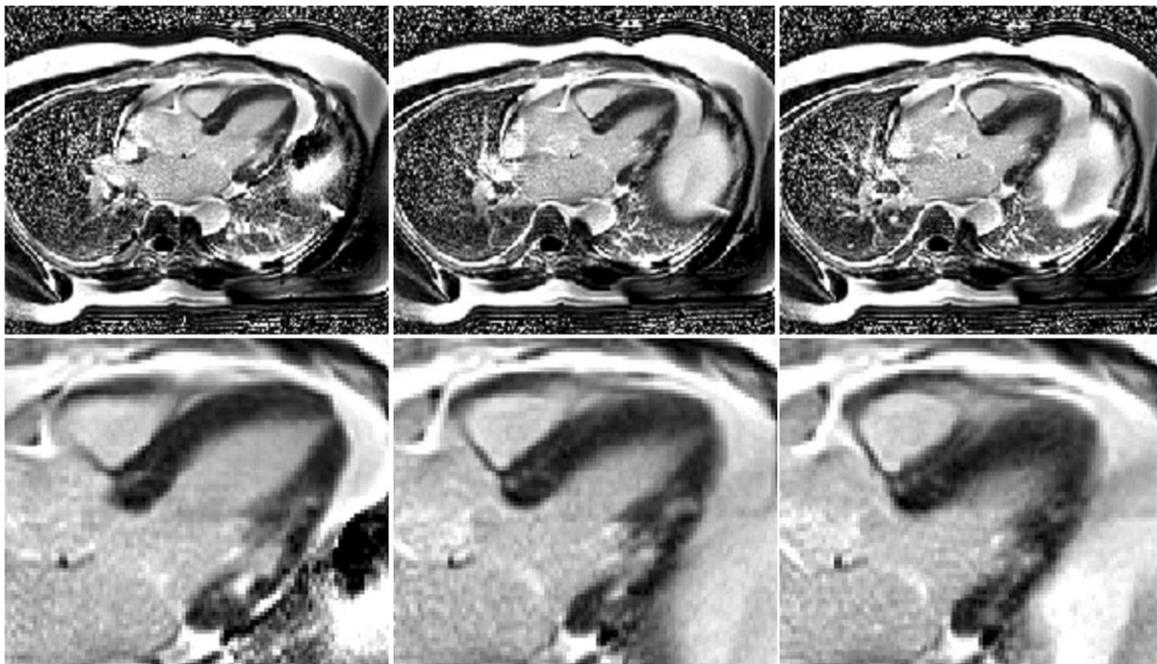
Figure 5. Motion-corrected averages of long-axis images acquired during free-breathing using nonrigid body image registration. The images shown represent 10 averages of the 30 images acquired corresponding to the minimum MSE starting with reference image 10 (left column), 11 (center column), and 12 (right column). The use of various consecutive reference images results in images at different respiratory positions. The choice of reference images was based on minimum MSE criteria.
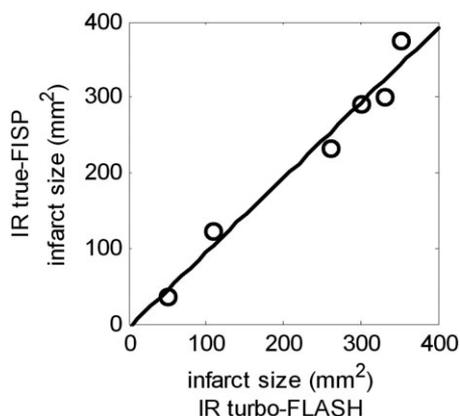
Figure 6. Comparison of infarct size measured in the motion-corrected averaged single-shot true-FISP and the conventional breathheld, segmented turbo-FLASH images.

posed a new method to make an automatic selection of the data to be averaged based on determining the best reference frames in terms of MSE. These reference images serve to produce three different averaged images corresponding to different respiratory phases, making optimal use of the original dataset. This strategy was used to discard nonuseful data with pronounced in-plane or out-of-plane motions, and may also be generalized for other applications. This approach effectively performs respiratory gating in a retrospective manner. As a generalized approach, the same strategy may be used for both short-axis and long-axis imaging. However, in our experience, the acceptance window for short-axis imaging may be made much higher. While this method has been predominantly evaluated only for midventricular short-axis slices, greater though-plane motion might be experienced in other slices. These cases may also require a reduced acceptance window. Currently, the acceptance window is determined as a user-defined parameter, although automatic determination may be possible.

The nonrigid-based scheme performed significantly better than rigid body registration in regions such as the RV where the motion of the RV is not generally the same as the LV used as a target in rigid body registration. There was no statistically significant difference in performance for the MI as measured for the six cases, although in some specific cases the MI edge profile had smaller variance for nonrigid registration. This is due to fact that the LV was well represented by rigid body motion for these patients. In some subjects, septal wall motion is observed with respiration. In these cases, the rigid body registration did not perform as well.

CONCLUSION

Motion-correction of free-breathing delayed-enhancement imaging using nonrigid image registration may be implemented in a fully automatic fashion and performs uniformly well across the full FOV. In prior work, it was shown that motion correction using rigid body registration performed well in comparison to conventional seg-

mented breathheld acquisition, in terms of MI size and contrast-to-noise ratio (CNR). The current work improves the performance across the whole heart to include the RV, and makes the method more practical by eliminating the need for user interaction to define the heart region. The MI as characterized by edge profiles was found to be at least as good as the rigid body case that has been previously validated. Therefore, in the same imaging time as required for a conventional breathheld segmented imaging approach, the proposed approach achieves delayed-enhancement images with high resolution and SNR without requiring a breath-hold. This is particularly attractive for cases in which patients have difficulty holding their breath. A new method to automatically find the best image frames to be averaged is also proposed to account for pronounced through-plane motion.

REFERENCES

1. Kim RJ, Fieno DS, Parrish TB, et al. Relationship of MRI delayed contrast enhancement to irreversible injury, infarct age, and contractile function. Circulation 1999;100:1992–2002.
2. Kim RJ, Wu E, Rafael A, et al. The use of contrast-enhanced magnetic resonance imaging to identify reversible myocardial dysfunction. N Engl J Med 2000;343:1445–1453.
3. Simonetti OP, Kim RJ, Fieno DS, et al. An improved MR imaging technique for the visualization of myocardial infarction. Radiology 2001;218:215–223.
4. Kim RJ, Shah DJ, Judd RM. How we perform delayed enhancement imaging. J Cardiovasc Magn Reson 2003;5:505–514.
5. Kellman P, Larson AC, Hsu LY, et al. Motion-corrected free-breathing delayed enhancement imaging of myocardial infarction. Magn Reson Med 2005;53:194–200.
6. Li W, Li BS, Polzin JA, Mai VM, Prasad PV, Edelman RR. Myocardial delayed enhancement imaging using inversion recovery single-shot steady-state free precession: initial experience. J Magn Reson Imaging 2004;20:327–330.
7. Huber A, Bauner K, Wintersperger BJ, et al. Phase-sensitive inversion recovery (PSIR) single-shot TrueFISP for assessment of myocardial infarction at 3 Tesla. Invest Radiol 2006;41:148–153.
8. Huber A, Schoenberg SO, Spannagl B, et al. Single-shot inversion recovery TrueFISP for assessment of myocardial infarction. AJR Am J Roentgenol 2006;186:627–633.
9. Chung Y, Vargas J, Simonetti O, Kim R, Judd R. Infarct imaging in a single heart beat. J Cardiovasc Magn Reson 2002;4:12–13.
10. Lee D, Wu E, Chung Y, et al. Comparison between single shot TrueFISP and segmented TurboFLASH for the detection of myocardial infarction. J Cardiovasc Magn Reson 2003;5:79–80.
11. Manke D, Nehrke K, Bornert P. Novel prospective respiratory motion correction approach for free-breathing coronary MR angiography using a patient-adapted affine motion model. Magn Reson Med 2003;50:122–131.
12. Manke D, Rosch P, Nehrke K, Bornert P, Dossel O. Model evaluation and calibration for prospective respiratory motion correction in coronary MR angiography based on 3-D image registration. IEEE Trans Med Imaging 2002;21:1132–1141.
13. McLeish K, Hill DLG, Atkinson D, Blackall JM, Razavi R. A study of the motion and deformation of the heart due to respiration. IEEE Trans Med Imaging 2002;21:1142–1150.
14. McLeish K, Kozerke S, Crum WR, Hill DLG. Free-breathing radial acquisitions of the heart. Magn Reson Med 2004;52:1127–1135.
15. Sorzano CO, Thevenaz P, Unser M. Elastic registration of biological images using vector-spline regularization. IEEE Trans Biomed Eng 2005;52:652–663.
16. Unser M, Aldroubi A, Eden M. The L(2) polynomial spline pyramid. IEEE Trans Pattern Anal Mach Intell 1993;15:364–379.
17. Kybic J, Unser M. Fast parametric elastic image registration. IEEE Trans Image Process 2003;12:1427–1442.

18. Ledesma-Carbayo MJ, Mahia-Casado P, Santos A, Perez-David E, Garcia-Fernandez MA, Desco M. Cardiac motion analysis from ultrasound sequences using nonrigid registration: validation against Doppler tissue velocity. Ultrasound Med Biol 2006;32: 483–490.

19. Thevenaz P, Ruttimann UE, Unser M. A pyramid approach to sub-pixel registration based on intensity. IEEE Trans Image Process 1998;7:27–41.

20. Hsu LY, Ingkanisorn WP, Kellman P, Aletras AH, Arai AE. Quantitative myocardial infarction on delayed enhancement MRI. Part II: Clinical application of an automated feature analysis and combined thresholding infarct sizing algorithm. J Magn Reson Imaging 2006;23:309–314.

21. Hsu LY, Natanzon A, Kellman P, Hirsch GA, Aletras AH, Arai AE. Quantitative myocardial infarction on delayed enhancement MRI. Part I: Animal validation of an automated feature analysis and combined thresholding infarct sizing algorithm. J Magn Reson Imaging 2006;23:298–308.

22. Maintz JB, Viergever MA. A survey of medical image registration. Med Image Anal 1998;2:1–36.

23. Rohlfing T, Maurer CR Jr, O'Dell WG, Zhong J. Modeling liver motion and deformation during the respiratory cycle using intensity-based nonrigid registration of gated MR images. Med Phys 2004;31:427–432.

24. Blackall JM, Penney GP, King AP, Hawkes DJ. Alignment of sparse freehand 3-D ultrasound with preoperative images of the liver using models of respiratory motion and deformation. IEEE Trans Med Imaging 2005;24:1405–1416.

25. Lamare F, Carbayo MJL, Kontaxakis G, et al. Incorporation of elastic transformations in list-mode based reconstruction for respiratory motion correction in PET. IEEE Nuclear Science Symposium Conference Record; 2005:1740–1744.